Inorganic Chemistry

Article

pubs.acs.org/IC

Porous Titania with Heavily Self-Doped Ti^{3+} for Specific Sensing of CO at Room Temperature

Juan Su,[†,‡] Xiao-Xin Zou,*[,†,‡] Yong-Cun Zou,[‡] Guo-Dong Li,[‡] Pei-Pei Wang,[‡] and Jie-Sheng Chen*[,†]

[†]School of Chemistry and Chemical Engineering, Shanghai Jiao Tong University, Shanghai 200240, P. R. China

[‡]State Key Laboratory of Inorganic Synthesis and Preparative Chemistry, Jilin University, Changchun 130012, P. R. China

Supporting Information

ABSTRACT: Semiconductor-based sensors have played an important role in efficient detection of combustible, flammable, and toxic gases, but they usually need to operate at elevated temperatures (200 °C or higher). Although reducing the operation temperature down to room temperature is of practical significance, it is still a huge challenge to fabricate room temperature sensors with a low cost. Here we show a novel "*self-doping*" strategy to overcome simultaneously both difficulties of "high resistance" and "low reaction rate", which have always been encountered for room-temperature operation of semiconductor-based sensors. In particular, a porous crystalline titania with heavily self-doped Ti^{3+} species has been prepared by using a porous amorphous TiO_2 and urea as the starting materials. The resulting Ti^{3+} self-doped TiO_2 material serves as an efficient room-temperature gas-sensing material for specific CO detection with fast response/recovery. The self-dopant (Ti^{3+}) in the titania material has proved to decrease the resistance of TiO_2 significantly on the one hand and to increase the chemisorbed oxygen species substantially, thus enhancing the surface reaction activity on the other. Such a self-doping concept is anticipated to give a fresh impetus to rational design of room-temperature sensing devices with low costs.

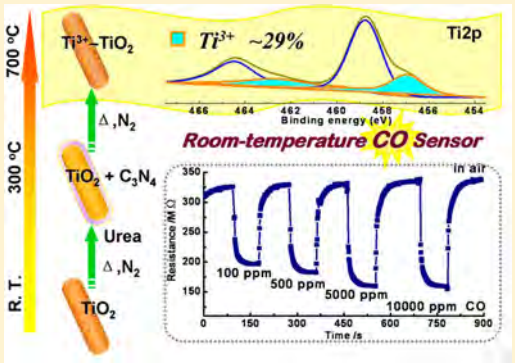

INTRODUCTION

Efficient detection of combustible, flammable, and toxic gases is highly desirable in industry and in daily lives of human beings. Practical gas detection relies on effective gas sensors, which are both highly safe and of low cost. Among the commercially available gas sensors, those based on semiconductor sensing materials are the most widely used because of their low cost, stability, and portability.[1] The fundamental mechanism of semiconductor sensors hinges on the interaction between the chemisorbed oxygen species on the sensor surface and the gas molecules to be detected, which leads to observable variation in the electrical resistance of the sensing material. Metal oxides such as SnO_2,[2−5] ZnO,[6−8] TiO_2,[9−11] and WO_3[12−14] have been extensively investigated as semiconductor sensing materials because of their good performance and low cost. However, sensors made of these compounds and other oxide materials usually need to operate at elevated temperatures (200 °C or higher).[1−14] Undoubtedly, reducing the operation temperature down to room temperature will further advance the widespread applications of oxide sensors because realization of room-temperature sensing simplifies the sensor fabrication process, reduces production cost (no heating element needed) and energy consumption, and increases operation safety (especially when elevated temperatures may trigger explosions). However, room-temperature operation of oxide sensors has always encountered two inherent difficulties.[15] First, the intrinsic resistance of oxide semiconductors is too high at room temperature and is usually beyond the detection limit. Second, the reaction kinetics, which is associated with the surface interaction between the chemisorbed oxygen species and the targeted gas molecules, is too slow at room temperature to give an obvious resistance change and quick response. As a result, elevated operation temperatures are usually necessary to decrease the resistance of oxide semiconductors and to increase the reaction kinetics.

Recently, research efforts have been devoted to exploration of room-temperature sensors through conductivity and surface-interaction enhancement of sensing materials.[15−24] For instance, the combination of SnO_2 nanoparticles with carbon nanotubes led to the realization of room-temperature sensing, thanks to the high adsorption capacity and conductivity of carbon nanotubes.[15] With assistance of UV-light irradiation, a single SnO_2 nanobelt can serve as a room-temperature sensing material with improved desorption kinetics.[18] However, there are at least two issues, poor selectivity and low response rate, that have limited optimization of the existing room-temperature sensors. The former renders the response of a sensor toward the monitored gas unreliable, whereas the latter leads to delay of sensing output.

Herein, we present a novel "*self-doping*" strategy to overcome simultaneously difficulties of both "high resistance" and "low

Received: January 15, 2013
Published: May 7, 2013

   dx.doi.org/10.1021/ic400109j | *Inorg. Chem.* 2013, 52, 5924−5930

reaction rate". In particular, a porous titania with heavily self-doped Ti^{3+} species (denoted hereafter as Ti^{3+}−TiO_2) has been prepared, and the resulting material functions as an efficient room-temperature gas-sensing material for CO detection with high selectivity and fast response/recovery. The self-dopant (Ti^{3+}) in the titania material has proved to decrease the resistance of TiO_2 on the one hand and to increase the chemisorbed oxygen species, thus enhancing the surface reaction activity on the other. In view that CO gas is extremely flammable and toxic, room-temperature sensors for selective and quick detection of CO have long been desired, and our strategy makes the easy fabrication of such sensors highly realizable.

EXPERIMENTAL SECTION

Materials. All chemical reagents used in our experiments were of analytical grade. Titanium *n*-butoxide and ethylene glycol were purchased from Tianjin Guangfu Fine Chemical Research Institute. Urea was purchased from Shantou Xilong Chemical Factory Co., Ltd.

Preparation of Ti^{3+}−TiO_2. For the preparation of Ti^{3+}−TiO_2, a porous amorphous TiO_2 and urea were used as the starting materials. This porous TiO_2 precursor was prepared by a light-driven synthetic method,[25] and the corresponding experimental details are provided in the Experimental Section in the Supporting Information (SI). Typically, a mixture of the porous amorphous TiO_2 precursor (0.32 g, 4.0 mmol) and urea (1 g, 16.7 mmol) was fully ground, followed by heating from room temperature to 700 °C (temperature ramp 1 °C/min) in a tube furnace under a nitrogen atmosphere. The heating temperature of 700 °C was then kept for 10 h before cooling down to room temperature to obtain the final solid product. To confirm the conversion of urea into C_3N_4 during the formation process of Ti^{3+}−TiO_2, a sample was obtained by heating the mixture of the porous amorphous TiO_2 precursor and urea at 300 °C. For comparison, another TiO_2 sample (TiO_2-300) was prepared by a low-temperature treatment (300 °C) of the Ti^{3+}−TiO_2 in air for 3 h. This sample was used as a reference for sensing property investigation.

General Characterization. The powder X-ray diffraction (XRD) patterns were recorded on a Rigaku D/Max 2550 X-ray diffractometer with Cu Kα radiation (λ = 1.5418 Å). The X-ray photoelectron spectroscopy (XPS) was performed on an ESCALAB 250 X-ray photoelectron spectrometer with a monochromatized X-ray source (Al Kα $h\nu$ = 1486.6 eV). The energy scale of the spectrometer was calibrated using Au $4f_{7/2}$, Cu $2p_{3/2}$, and Ag $3d_{5/2}$ peak positions. The standard deviation for the binding energy values is 0.1 eV. The scanning electron microscopy (SEM) images were taken on a JEOL JSM 6700F electron microscope. The FT-IR spectra were acquired on a Bruker IFS 66v/S FT-IR spectrometer. The nitrogen adsorption and desorption isotherms were measured using a Micromeritics ASAP 2020 M system. The TEM images were obtained on a JEOL JSM-3010 TEM microscope. The thermogravimetric (TG) analysis was performed in N_2 on a Netzsch STA 449C TG thermal analyzer from 25 to 800 °C at a heating rate of 10 °C min^{-1}. The nitrogen adsorption and desorption isotherms were measured by using a Micromeritics ASAP 2020 M system. Prior to each measurement, the sample was evacuated at 300 K for 12 h to remove the adsorbed guest species, such as water. The surface area data were calculated on the basis of the Brunauer−Emmett−Teller (BET) model. The conductivities of the TiO_2 samples were measured by the standard four-probe method at room temperature. The details of the sample treatment were as follows: first, the powdered sample was ground for 20 min and was pressed into small disks with a diameter of 1 cm and a thickness of 3 mm. Then, the disks were heated at 600 °C for 24 h under N_2 protection. Finally, prior to measurement, the surfaces of the disks were coated with air-drying conducting silver paste (BQ-6880E, Uninwell International) and cured at room temperature for 24 h. The O_2 temperature programmed desorption (O_2-TPD) was performed using an Automated Catalyst Characterization System (AutoChem II 2920 V3.05, Micromeritics Instrument Corporation). For a typical TPD experiment, 100 mg of sample was pretreated under a flow of 10% O_2 in Ar (20 mL/min) at room temperature (about 25 °C) for 2 h and then swept by a He flow of 30 mL/min for 2 h. The O_2-TPD was performed with a temperature ramp of 5 °C/min from 25 to 100 °C under a He flow of 10 mL/min. The oxygen amount was monitored and quantified on a gas chromatograph using a thermal conductivity detector.

Room-Temperature Sensor Fabrication and Testing. The gas sensor was fabricated by pasting a viscous slurry of the obtained sample onto an alumina tube with a diameter of 1 mm and a length of 4 mm, which was positioned with a pair of Au electrodes and four Pt wires on both ends of the tube (Figure S1a in the SI). No heating element was needed for the sensor fabrication. It should be noted that Pt wires were chosen as conducting wires because of their excellent conductivity and stability. In addition, although Pt is a well-known catalyst, Pt wires used herein did not affect the behavior of the material because there was no direct contact between Pt wires and the sensing films. Gas sensing tests were performed on a commercial CGS-8 Gas Sensing Measurement System (Beijing Elite Tech Company Limited). The upper detection limit of resistance in this system was set to 500 MΩ. This detection limit of resistance ensures the following: (1) the working voltage is not too large, and thereby the sensor cannot be burnt out; (2) the signal current is not too small, and the signal noise is not too large. In the system, a load resistor was connected in series with the sensor, and Figure S1b in the SI shows the working principle of this system. The resistance (or output voltage, V_{out}) of a sensor in air or a target gas was measured by monitoring the terminal voltage of the load resistor at a test circuit voltage of 5 V (V_c).

Gas sensing properties were measured using a static test system which included a test chamber (~1 L in volume) at room temperature (25 ± 3 °C). Environmental air with a relative humidity of 15−20% was used as both a reference gas and a diluting gas to obtain the desired concentrations of target gases. A typical testing procedure was as follows. After the target gas was injected into the test chamber by a syringe, the sensor was put into the test chamber. When the response reached a constant value, the sensor was taken out to recover in air. The response and recovery times for the sensor are defined as the times taken by the sensor to achieve 90% of the total resistance change.

RESULTS AND DISCUSSION

Preparation and Characterization of Ti^{3+}−TiO_2. For the preparation of Ti^{3+}−TiO_2, a porous amorphous TiO_2 sample and urea were chosen as the starting materials. This porous TiO_2 precursor was obtained through a light-driven synthetic method,[25] and the BET surface area of the resulting material was 530 m^2/g (the corresponding experimental details are provided in the Experimental Section). The use of the porous amorphous TiO_2 as precursor was because it could activate urea to form carbon nitride (C_3N_4) under mild conditions,[26] and it led to a porous final product. The Ti^{3+}−TiO_2 material was easily synthesized through heating a mixture of the porous amorphous TiO_2 precursor and urea at 700 °C in a nitrogen atmosphere, as shown in Figure 1. With the increase of reaction temperature from room temperature to 700 °C, urea is first converted to carbon nitride at around 300 °C under the assistance of the porous TiO_2 precursor (Figure S2 in the SI),[26] which in turn is coated by the as-formed C_3N_4. When the temperature is elevated to 700 °C, the as-formed C_3N_4 decomposes and reacts with the porous TiO_2, leading to the formation of Ti^{3+}−TiO_2 with a porous crystalline structure. The whole preparation process is rather facile, reproducible, and economically viable because urea, the only species consumed, is abundant and cheap.

At 300 °C, the conversion of urea into C_3N_4 has been confirmed by powder XRD (Figure S3 in the SI) and FT-IR spectroscopy (Figure S4 in the SI). Note that at this

dx.doi.org/10.1021/ic400109j | Inorg. Chem. 2013, 52, 5924−5930

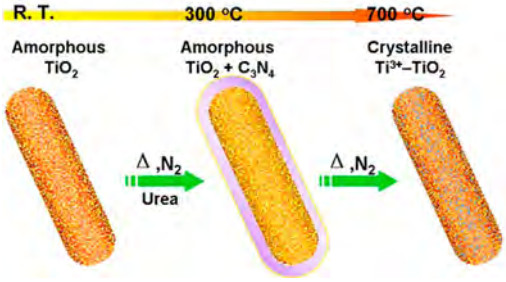

Figure 1. Schematic representation for the preparation of Ti^{3+}–TiO_2 using porous amorphous TiO_2 and urea as starting materials. With the increase of reaction temperature from room temperature (RT) to 700 °C, urea first converts into C_3N_4 on the TiO_2 surface at around 300 °C, and then the as-formed C_3N_4 totally decomposes at 700 °C and reacts with the porous TiO_2, leading to the formation of Ti^{3+}–TiO_2 with a crystalline structure.

temperature the porous TiO_2 precursor still remains amorphous. Scanning electron microscopy (Figure S5 in the SI) and transmission electron microscopy (TEM, Figure S6 in the SI) show that the surface of the porous TiO_2 particles is fully coated by the as-formed C_3N_4 after the treatment at 300 °C. This observation is further supported by the N_2 adsorption measurement results. The C_3N_4-coated TiO_2 loses the porosity of the TiO_2 precursor, and its BET surface area is reduced to only 11.8 m^2/g. In contrast, the TiO_2 sample obtained by direct thermal treatment of the porous TiO_2 precursor at 300 °C in the absence of urea possesses a BET surface area of ~300 m^2/g. The TG analysis for the C_3N_4-coated TiO_2 was performed in N_2 from 25 to 800 °C, and the corresponding TG curve is shown in Figure S7 in the SI. It is seen that an obvious weight loss of 56.6% ends at about 650 °C, indicating the complete decomposition of C_3N_4 above this temperature.

On the basis of the TG analysis, a final reaction temperature of 700 °C was chosen to ensure that the C_3N_4 was completely removed from the solid product of the Ti^{3+}–TiO_2 material. Figure 2 shows the powder XRD pattern of the Ti^{3+}–TiO_2

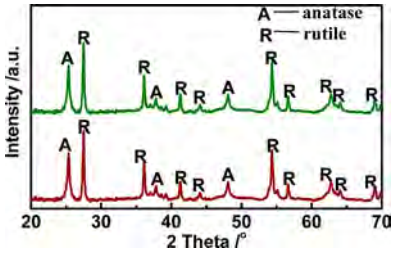

Figure 2. XRD patterns of Ti^{3+}–TiO_2 (red line) and TiO_2-300 (green line).

sample obtained at 700 °C. It is seen that the diffraction peaks associated with the C_3N_4 intermediate (Figure S3 in the SI) completely disappear, and no impurity phases, such as titanium carbides and nitrides, are observed apart from the anatase and the rutile TiO_2. Calculation based on the anatase (101) and rutile (110) peak intensities[27] (Figure 2) indicates that the anatase and rutile contents in the Ti^{3+}–TiO_2 material are about 37.1 and 62.9 wt %, respectively. The complete decomposition of the C_3N_4 intermediate is also confirmed by FT-IR (Figure S8 in the SI), SEM (Figure S9 in the SI), and TEM (Figure 3) characterizations. In comparison with the C_3N_4-coated TiO_2 (Figure S6), the Ti^{3+}–TiO_2 material does not show any

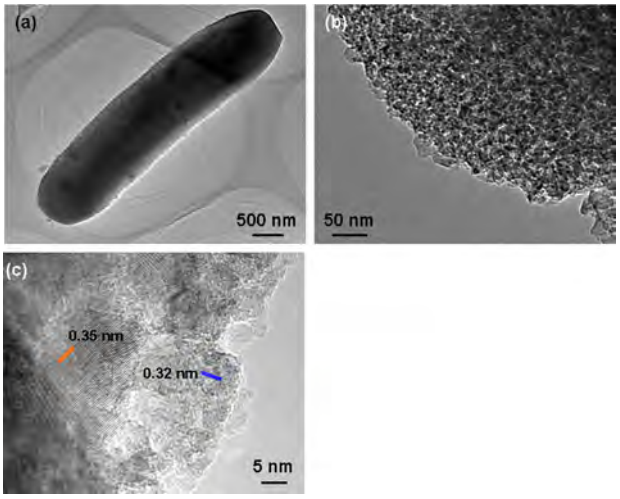

Figure 3. (a, b) TEM and (c) HRTEM images of Ti^{3+}–TiO_2.

observable C_3N_4 phase (Figure 3a and b), confirming the complete decomposition of C_3N_4 at 700 °C. The HRTEM image (Figure 3c) shows that the Ti^{3+}–TiO_2 material is highly crystalline. The observed lattice spacings are 0.35 and 0.32 nm, which correspond to interplanar distances of the (101) crystal planes for the anatase TiO_2 and the (110) crystal planes for rutile TiO_2, respectively.

The N_2 adsorption/desorption isotherms (Figure 4a) of Ti^{3+}–TiO_2 exhibit a characteristic type-IV curve with an H1

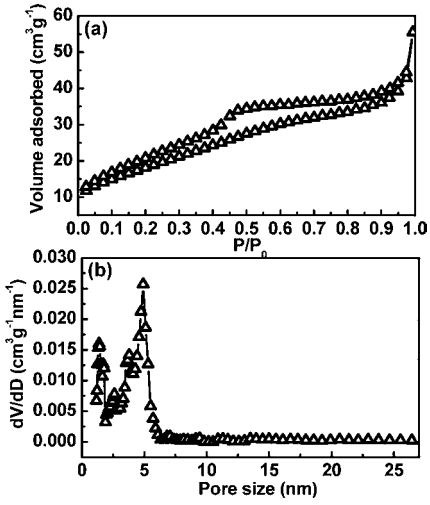

Figure 4. (a) N_2 adsorption/desorption isotherms for Ti^{3+}–TiO_2; and (b) its corresponding pore-size distribution.

hysteresis loop, indicative of mesoporous feature. The Barrett–Joyner–Harlenda pore-size distribution of the material calculated on the basis of the adsorption branch of the isotherm (Figure 4b) reveals a narrow pore-size distribution, ranging from 1.2 to 6.3 nm. The corresponding BET surface area of the material is found to be 67 m^2/g. Obviously, the as-obtained Ti^{3+}–TiO_2 material has a surface area much smaller than the amorphous porous TiO_2 precursor (530 m^2/g). Although the Ti^{3+}–TiO_2 material possesses only a modest surface area (67 m^2/g), the porous structure makes it suitable for sensing application because sensing events occur on the surface of TiO_2.[1]

dx.doi.org/10.1021/ic400109j | Inorg. Chem. 2013, 52, 5924–5930

To obtain the information about the composition of Ti^{3+}–TiO_2, XPS was performed. The Ti 2p spectrum (Figure 5) gives

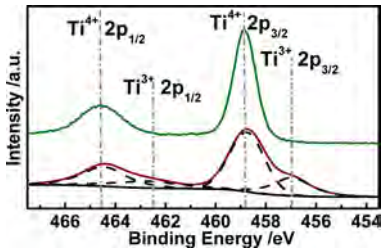

Figure 5. Ti 2p XPS spectra of Ti^{3+}–TiO_2 (red line) and TiO_2-300 (green line).

the Ti $2p_{3/2}$ and Ti $2p_{1/2}$ binding energies ranging from 455 to 461 eV and from 461 to 467 eV, respectively. The fitting for the Ti $2p_{3/2}$ peak reveals the presence of a major peak at 458.8 eV with a shoulder at 456.8 eV. The Ti $2p_{1/2}$ peak is also deconvoluted into two components with binding energies at 464.6 and 462.5 eV. The peaks at 458.8 and 464.6 eV are assigned to the $2p_{3/2}$ and $2p_{1/2}$ core levels of Ti^{4+}, whereas the peaks at 456.8 and 462.5 eV are attributable to the $2p_{3/2}$ and $2p_{1/2}$ core levels of Ti^{3+}, respectively. The quantitative analysis of the XPS data indicates that the $Ti^{3+}/(Ti^{3+} + Ti^{4+})$ atomic ratio is about 0.29:1.00; that is, 29% of the titanium species in Ti^{3+}–TiO_2 are present in the form of Ti^{3+}. The formation of Ti^{3+} in TiO_2 is attributed to the reducing action of C_3N_4 that coats the surface of the TiO_2 particles. The decomposition of C_3N_4 at 700 °C generates highly reactive carbon and nitrogen species, the interaction of which with TiO_2 leads to oxygen deficiency in the latter. During this process, electrons are transferred from the reducing species associated with C_3N_4 to the Ti^{4+} cations to form Ti^{3+} cations. It is generally presumed that Ti^{3+}, if accessible, can be easily oxidized by O_2 to form Ti^{4+}, but the Ti^{3+}–TiO_2 material remains stable in air (its Ti^{3+} is not oxidized by O_2) for a time as long as twelve months at room temperature. The excellent stability of Ti^{3+}–TiO_2 indicates that the Ti^{3+} species are present in the bulk or at the subsurface, rather than on the surface of the TiO_2 particles. Because the detection depth of the XPS measurement is about 5 nm, it is certain that there are abundant Ti^{3+} species at the subsurface of the TiO_2 particles. The excellent stability and high subsurface Ti^{3+} content of Ti^{3+}–TiO_2 prompted us to exploit this material for room-temperature sensing applications.

The possible presence of nitrogen and carbon dopants in Ti^{3+}–TiO_2 was examined by the N 1s and C 1s XPS (Figure 6). A nitrogen peak at 396.5 eV and a carbon peak at 284.8 eV were detected for Ti^{3+}–TiO_2. The position of the nitrogen peak (396.5 eV) is in the range (396–404 eV) previously observed in nitrogen-doped TiO_2.[28] The carbon peak at 284.8 eV is assigned to the elemental carbon. Therefore, it is presumable that, during the formation of Ti^{3+}–TiO_2, nitrogen is doped into the titania particles and a tiny amount of residual carbon is possibly present. For comparison purposes, thermal treatment of Ti^{3+}–TiO_2 at 300 °C in air was carefully performed to ensure that the Ti^{3+} species in the material were oxidized whereas the nitrogen and carbon species were retained. The sample (designated TiO_2-300) obtained after this treatment was used as a reference for structure and property investigation. As shown in Figure 5, the Ti^{3+}-related signals in the XPS spectrum of TiO_2-300 disappear completely, indicating the conversion of Ti^{3+} to Ti^{4+} in Ti^{3+}–TiO_2 after the thermal

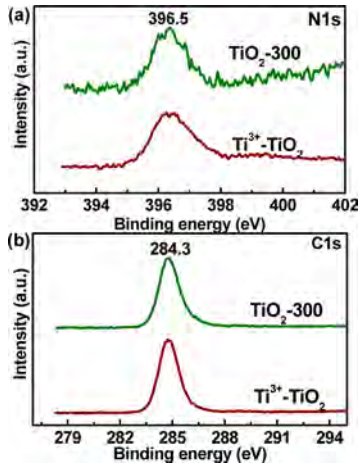

Figure 6. (a) N 1s and (b) C 1s XPS spectra for Ti^{3+}–TiO_2 (red line) and TiO_2-300 (green line) .

treatment. However, the thermal treatment does not lead to crystal structure variation, as the XRD pattern of TiO_2-300 is identical to that of the as-prepared Ti^{3+}–TiO_2 material (see Figure 2). On the other hand, the nitrogen and carbon species in the Ti^{3+}–TiO_2 sample is maintained after the thermal treatment, as demonstrated by the XPS measurement (see Figure 6). On the basis of the above results, it is concluded that the only difference between Ti^{3+}–TiO_2 and TiO_2-300 lies in the presence (or absence) of Ti^{3+} species in the two samples.

Previously, titania samples with Ti^{3+} species were obtained by different synthetic methods,[25,29–38] and they were already reported to serve as photocatalytic materials,[29–33] photoelectric conversion materials,[34,35] ferromagnetic materials,[25,36,37] biomaterials,[38] and so on. It was confirmed that the presence of Ti^{3+} plays an important role in enhancing the performances of the TiO_2 materials.[25,29–38] Nevertheless, no room-temperature sensing application of Ti^{3+}-containing TiO_2 materials has appeared in the literature at all. In some of the previously reported Ti^{3+}–TiO_2 materials,[25,36,37] the Ti^{3+} species are present on the surface of TiO_2 and thus are unstable toward air because the Ti^{3+} species can be easily oxidized by oxygen in air. Obviously, these air-unstable Ti^{3+}–TiO_2 materials are not suitable for sensing application. In other cases, the Ti^{3+}–TiO_2 materials are air-stable, but they still cannot be used for room-temperature sensing because the Ti^{3+} species in these materials are deeply buried in the bulk of the TiO_2 particles. Bulk Ti^{3+} cannot efficiently decrease the electric resistance and increase the surface reaction activity of TiO_2, as demonstrated by the fact that a bulk self-doped TiO_2 material shows sensing behavior only at 300 °C.[11] The Ti^{3+}–TiO_2 material reported herein is unique because it contains a considerable proportion of Ti^{3+} in the subsurface region of the titania particles. The material is air-stable, and more importantly, it exhibits room-temperature sensing properties (see below).

Room-Temperature Sensing of Ti^{3+}–TiO_2. As mentioned earlier, there are two inherent difficulties—"high resistance" and "low reaction rate"—associated with semiconductor sensing materials at room temperature. In order to examine the abilities of the self-dopant Ti^{3+} in TiO_2 to overcome these two difficulties, the room-temperature electrical conductivity of Ti^{3+}–TiO_2 was measured through the standard four-point probe method, and the room-temperature chemical O_2 adsorption property of Ti^{3+}–TiO_2 was studied by the O_2-

dx.doi.org/10.1021/ic400109j | Inorg. Chem. 2013, 52, 5924–5930

TPD measurement. Figure 7a presents the comparison of the electrical conductivities of Ti^{3+}−TiO_2 and TiO_2-300. It is seen

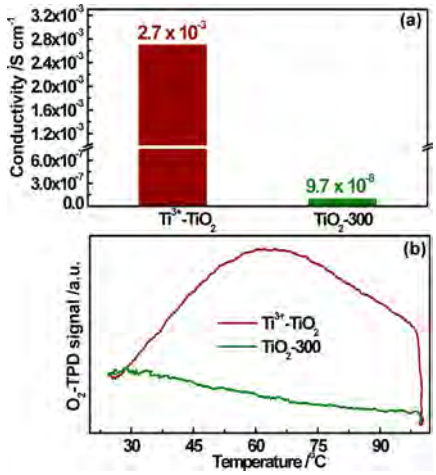

Figure 7. (a) Comparison of the electrical conductivities of Ti^{3+}−TiO_2 (red) and TiO_2-300 (green). (b) Comparison of the chemical O_2 adsorption properties of Ti^{3+}−TiO_2 (red line) and TiO_2-300 (green line).

that Ti^{3+}−TiO_2 exhibits a conductivity value of 2.7×10^{-3} S/cm whereas the conductivity value of the TiO_2-300 sample is merely 9.7×10^{-8} S/cm. In other words, the resistance of Ti^{3+}−TiO_2 decreases by ~5 orders of magnitude in comparison with that of TiO_2-300 due to the presence of Ti^{3+}. The improvement in electrical conductivity (or the decrease in resistance) of TiO_2 by Ti^{3+} self-doping is because Ti^{3+} species in TiO_2 can function as efficient donors, the electrons of which can hop to the conduction band (or adjacent Ti^{4+} sites).[39,40] Figure 7b shows the chemical O_2 adsorption properties of Ti^{3+}−TiO_2 and TiO_2-300. Differing from the TiO_2-300 material with almost no chemisorbed O_2 on its surface, Ti^{3+}−TiO_2 exhibits a substantial increase of the chemisorbed oxygen species (25.2 mmol/g of TiO_2).

Given the unique dual functions of Ti^{3+} in TiO_2, it is expected that Ti^{3+}−TiO_2 would serve as a good room-temperature sensing material. A typical sensor was fabricated conveniently by pasting a slurry of the Ti^{3+}−TiO_2 material onto a ceramic tube with a diameter of 1 mm and a length of 4 mm, which was positioned with a pair of Au electrodes and four Pt wires on both ends of the tube (Figure S1a in the SI). It should be noted that no heating element is needed for the sensor fabrication. The response and recovery times for the sensor are defined as the times taken by the sensor to achieve 90% of the total resistance change.

The performance of the sensor based on Ti^{3+}−TiO_2 was studied at room temperature by testing a wide range of gases and organic vapors. The experimental results show that the Ti^{3+}−TiO_2 sensor only responds to carbon monoxide and is totally insensitive to hydrogen, methane, ethylene, acetone, and methanol (Figure S10 in the SI), demonstrating the excellent selectivity of the Ti^{3+}−TiO_2 sensor. The unique selectivity toward CO gas is possibly attributed to the relatively stronger interaction between CO and surface-absorbed oxygen at low temperature.[41] However, the full understanding of the reasons behind this selectivity is very difficult because sensing is quite a complex chemical reaction process, which can be influenced by several factors, such as the adsorption amount, exciting type and sites of adsorbed oxygen and target gas on the oxide surface, and the interaction between them. This difficulty was always encountered in previous reports related to sensors with selectivity.[11,13,42,43] Considering the importance of selectivity for a sensor (especially in a complex and changing environment), further deep investigation, which is underway, of structure−selectivity correlations is needed, and the results will be reported elsewhere.

Figure 8a presents the dynamic response-recovery curve of the Ti^{3+}−TiO_2 sensor with increasing CO concentrations. It is

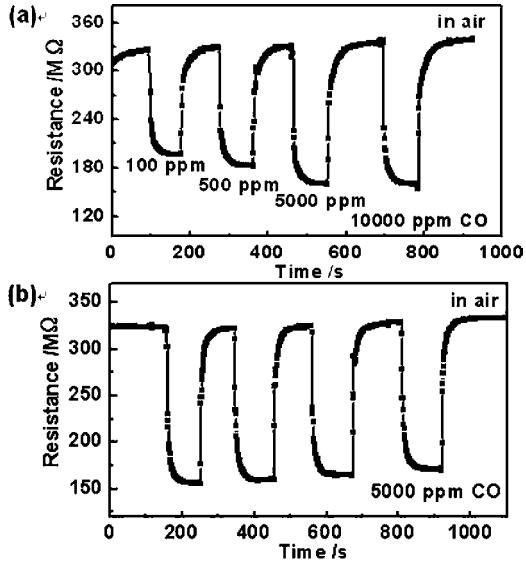

Figure 8. (a) Dynamic response-recovery curve of the Ti^{3+}−TiO_2 sensor with increasing CO concentrations. (b) Dynamic response-recovery curve of the Ti^{3+}−TiO_2 sensor for continuous detection in 5000 ppm CO.

seen that the sensor has a wide response range for CO gas from 100 to 10,000 ppm. When the sensor is exposed to 100 ppm CO, its resistance rapidly decreases from ~325 MΩ (in air) to ~198 MΩ, and the resistance returns quickly to the original value when the sensor is exposed to air again. Similar response and recovery behaviors are also observed for the detection of CO gas with a higher concentration, but a higher CO concentration results in a lower resistance. For CO concentrations of 500, 5,000, and 10,000 ppm, the resistances are about 182, 161, and 157 MΩ, respectively. In addition to the concentration-dependent response, the Ti^{3+}−TiO_2 sensor exhibits satisfactory signal stability. As shown in Figure 8b, four almost identical signals are observed in rapid succession in the presence of 5,000 ppm CO. Furthermore, the response and recovery times, which are also critical for a gas sensor, have been measured for the Ti^{3+}−TiO_2 sensor, and the results show that the response time is less than 10 s, and the recovery time is less than 30 s. From the above sensing results, it is concluded that the Ti^{3+}−TiO_2 material is very promising for the fabrication of a room-temperature CO sensor because of its high selectivity, high signal stability, as well as fast response and recovery.

Up to now, many oxide semiconductors, including SnO_2, ZnO, TiO_2, MoO_3, Co_3O_4, CuO, and In_2O_3, were explored as CO sensing materials at high operating temperature (>200 °C).[42,44] Several feasible strategies (e.g., surface modification with noble metal particles, bulk doping with heteroatoms, and

dx.doi.org/10.1021/ic400109j | Inorg. Chem. 2013, 52, 5924−5930

nanoscale structural design) were developed to enhance their sensing properties, such as sensitivity and/or selectivity. But these strategies were usually not effective for reducing the operation temperature down to room temperature.[42,44] Although three CO sensing materials working at room temperature (SnO_2−carbon nanotube composite,[15,16] porous SnO_2 nanowires,[24] and porous Co_3O_4 nanostructures[21]) were reported, these sensing materials showed poor selectivity and/or low response/recovery rates for CO detection. Thus, our Ti^{3+}−TiO_2 sensing material, which is achieved by a novel "self-doping" strategy, is advantageous among the CO sensing materials, in terms of combination of room-temperature operation, high selectivity, and fast response/recovery.

For comparison, three more gas sensors have also been fabricated from TiO_2-300, Ti^{3+}-free anatase, and Ti^{3+}-free rutile, and they have been tested for CO detection. At room temperature, the resistances of these three gas sensors based on Ti^{3+}-free TiO_2 materials are all beyond the detection limit (500 MΩ), and thereby they cannot be used for CO detection at room temperature. This result demonstrates that the resistance decrease by Ti^{3+} self-doping is important for the realization of room-temperature sensing based on titania material. In addition, considering the fact that the only difference between Ti^{3+}−TiO_2 and TiO_2-300 lies in the presence (or absence) of Ti^{3+} species in the two samples (as mentioned earlier), Ti^{3+} species, rather than other structural feature (e.g., porous structure), play a crucial role in the room-temperature properties of Ti^{3+}−TiO_2. The porous structure (or high surface area) might only have some auxiliary effects on gas sensing performance, such as increasing the surface reactive sites and facilitating the diffusion of target gases. Furthermore, even if the resistances of the Ti^{3+}-free TiO_2 sensors are made to be within the detection limit by increasing the operating temperature to 300 °C, the sensors still have no response to CO gas. Apparently, the function of the Ti^{3+} self-doping is more than just decreasing the resistance of TiO_2 down to the detection limit. The oxygen adsorption is also substantially enhanced by the Ti^{3+} self-doping, and this oxygen adsorption enhancement equally contributes to the excellent room-temperature sensing performance of the Ti^{3+}−TiO_2 material.

The sensing mechanism of Ti^{3+}−TiO_2 (Figure 9) is associated with the interaction of surface chemisorbed oxygen and the CO gas at room temperature.[1] The oxygen molecules in air are chemisorbed on the TiO_2 surface and then extract electrons from the TiO_2 surface, leading to the formation of a depletion layer. The depletion layer gives rise to a potential barrier and thus a high-resistance state. When the sensor is exposed to CO gas, the latter reacts with the surface oxygen species, and correspondingly the amount of surface adsorbed oxygen decreases to a certain extent. As a result, the height of the potential barrier is reduced, and the resistance of the whole sensing layer decreases significantly. For such a surface reaction, the increase in amount of surface-adsorbed oxygen is beneficial to the reaction activity/kinetics, or it allows for fast oxidation of the CO gas on the TiO_2 surface. In addition, the decrease in electrical resistance not only makes it feasible to detect the resistance (and its variation) for a room-temperature sensor but also enables the rapid electron transport between the Au electrodes of the sensor. Therefore, the simultaneous accomplishment of high oxygen adsorption and low electrical resistance by the Ti^{3+} self-doping plays a crucial role in the room-temperature sensing performance of the Ti^{3+}−TiO_2 material.

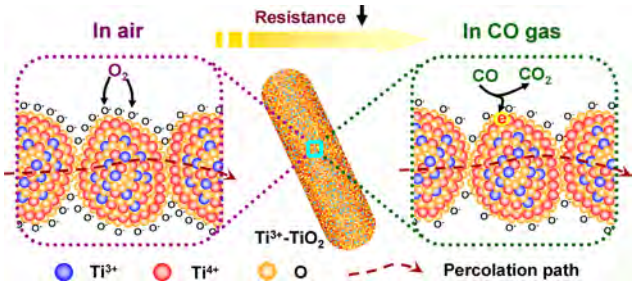

Figure 9. Schematic representation of the sensing mechanism of Ti^{3+}−TiO_2. Resistance ↓ means resistance decrease. Percolation path means electron transport pathway between the Au electrodes of the sensor.

CONCLUSIONS

In summary, we present a novel *Ti^{3+} self-doping* strategy for fabrication of a room-temperature sensor based on an inexpensive TiO_2 semiconductor. Using a porous amorphous TiO_2 and urea as the starting materials, a porous titania with heavily self-doped Ti^{3+} (Ti^{3+}−TiO_2) has been successfully prepared, and the obtained compound serves as an efficient room-temperature gas-sensing material for specific CO detection with fast response/recovery. The Ti^{3+} self-doping has proved to be fundamental for achievement of room-temperature sensing of the TiO_2 sensor. The Ti^{3+} dopant in TiO_2 not only decreases the resistance of TiO_2 significantly but also enhances the surface reaction activity by increasing the chemisorbed oxygen species on the TiO_2 surface to a great extent. The deep understanding of Ti^{3+}−property correlations, beyond doubt, will be beneficial for further development of a wide range of Ti^{3+}-related applications. Such a *self-doping* concept may be extended to other oxide semiconductors besides TiO_2, providing new opportunities for fabrication of advanced devices with low costs.

ASSOCIATED CONTENT

Supporting Information

Synthesis of the porous amorphous TiO_2 precursor, photograph of a gas sensor, schematic diagram of the measurement circuit, scheme for the formation of the C_3N_4 intermediate, TEM image, SEM images, TG curve, XRD pattern and IR spectrum of C_3N_4-coated porous TiO_2, SEM images of amorphous TiO_2 and Ti^{3+}−TiO_2, IR spectrum of Ti^{3+}−TiO_2, dynamic response-recovery curves of the Ti^{3+}−TiO_2 sensor with increasing concentrations of different gases. This material is available free of charge via the Internet at http://pubs.acs.org.

AUTHOR INFORMATION

Corresponding Author

*E-mail: chem_zouxx@163.com (X.-X.Z.), chemcj@sjtu.edu.cn (J.-S.C.).

Notes

The authors declare no competing financial interest.

ACKNOWLEDGMENTS

This work was financially supported by the National Basic Research Program of China (2013CB934102, 2011CB808703) and the National Natural Science Foundation of China.

REFERENCES

(1) Franke, M. E.; Koplin, T. J.; Simon, U. *Small* **2006**, *2*, 36.
(2) Liu, Yi.; Koep, E.; Liu, M. *Chem. Mater.* **2005**, *17*, 3997.
(3) Kim, H.-R.; Haensch, A.; Kim, I.-D.; Barsan, N.; Weimar, U.; Lee, J.-H. *Adv. Funct. Mater.* **2011**, *21*, 4456.
(4) Kolmakov, A.; Zhang, Y.; Cheng, G.; Moskovits, M. *Adv. Mater.* **2003**, *15*, 997.
(5) Wang, B.; Zhu, L. F.; Yang, Y. H.; Xu, N. S.; Yang, G. W. *J. Phys. Chem. C* **2008**, *112*, 6643.
(6) Wan, Q.; Li, Q. H.; Chen, Y. J.; Wang, T. H.; He, X. L.; Li, J. P.; Lin, C. L. *Appl. Phys. Lett.* **2004**, *84*, 3654.
(7) Jing, Z.; Zhan, Ji. *Adv. Mater.* **2008**, *20*, 4547.
(8) Zou, X.-X.; Li, G.-D.; Zhao, J.; Wang, P.-P.; Wang, Y.-N.; Zhou, Li.-J.; Su, J.; Li, L.; Chen, J.-S. *Inorg. Chem.* **2011**, *50*, 9106.
(9) Zuruzi, A. S.; Kolmakov, A.; MacDonald, N. C.; Moskovits, M. *Appl. Phys. Lett.* **2006**, *88*, 102904.
(10) Kim, I.-D.; Rothschild, A.; Lee, B. H.; Kim, D. Y.; Jo, S. M.; Tuller, H. L. *Nano Lett.* **2006**, *6*, 2009.
(11) Zou, X.; Li, G.; Zou, Y.; Wang, P.; Su, J.; Zhao, J.; Wang, Y.; Chen, J. *Acta Chim. Sin.* **2012**, *70*, 1477.
(12) D'Arienzo, M.; Armelao, L.; Mari, C. M.; Polizzi, S.; Ruffo, R.; Scotti, R.; Morazzoni, Fr. *J. Am. Chem. Soc.* **2011**, *133*, 5296.
(13) Zou, X.-X.; Li, G.-D.; Wang, P.-P.; Su, J.; Zhao, J.; Zhou, L.-J.; Wang, Y.-N.; Chen, J. S. *Dalton Trans.* **2012**, *41*, 9773.
(14) Wang, G.; Ji, Y.; Huang, X.; Yang, X.; Gouma, P.; Dudley, M. *J. Phys. Chem. B* **2006**, *110*, 23777.
(15) Lu, G.; Ocola, L. E.; Chen, J. *Adv. Mater.* **2009**, *21*, 2487.
(16) Yang, A.; Tao, X.; Wang, R.; Lee, S.; Surya, C. *Appl. Phys. Lett.* **2007**, *91*, 133110.
(17) Wei, B.-Y.; Hsu, M.-C.; Su, P.-G.; Lin, H.-M; Wu, R.-J.; Lai, H.-J. *Sens. Actuators, B* **2004**, *101*, 81.
(18) Law, M.; Kind, H.; Messer, B.; Kim, F.; Yang, P. D. *Angew. Chem.* **2002**, *114*, 2511.
(19) Comini, E.; Cristalli, A.; Faglia, G.; Sberveglieri, G. *Sens. Actuators, B* **2000**, *65*, 260.
(20) (a) Liu, Z.; Yamazaki, T.; Shen, Y.; Kikuta, T.; Nakatani, N.; Kawabata, T. *Appl. Phys. Lett.* **2007**, *90*, 173119. (b) Mor, G. K.; Carvalho, M. A.; Varghese, O. K.; Pishko, M. V.; Grimes, C. A. *J. Mater. Res.* **2004**, *19*, 628.
(21) Geng, B.; Zhan, F.; Fang, C.; Yu, Na. *J. Mater. Chem.* **2008**, *18*, 4977.
(22) Patil, D. R.; Patil, L. A. *Sens. Actuators, B* **2007**, *123*, 546.
(23) Kim, Y. S.; Ha, S.-C.; Kim, K.; Yang, H.; Choi, S.-Y.; Kim, Y. T.; Park, J. T.; Lee, C. H.; Choi, J.; Paek, J.; Leea, K. *Appl. Phys. Lett.* **2005**, *86*, 213105.
(24) Wang, Y.; Jiang, Xu.; Xia, Y. *J. Am. Chem. Soc.* **2003**, *125*, 16176.
(25) Zou, X.-X.; Li, G.-D.; Wang, K.-X.; Li, L.; Su, J.; Chen, J.-S. *Chem. Commun.* **2010**, *46*, 2112.
(26) Zou, X.-X.; Li, G.-D.; Wang, Y.-N.; Zhao, J.; Yan, C.; Guo, M.-Y.; Li, L.; Chen, J.-S. *Chem. Commun.* **2011**, *47*, 1066.
(27) Luo, H.; Wang, C.; Yan, Y. *Chem. Mater.* **2003**, *15*, 3841.
(28) Wu, Y.; Liu, H.; Zhang, J.; Chen, F. *J. Phys. Chem. C* **2009**, *113*, 14689.
(29) Hamdy, M. S.; Amrollahi, R.; Mul, G. *ACS Catal.* **2012**, *2*, 2641.
(30) Sayed, F. N.; Jayakumar, O. D.; Sasikala, R.; Kadam, R. M.; Bharadwaj, S. R.; Kienle, L.; Schürmann, U.; Kaps, S.; Adelung, Ra.; Mittal, J. P.; Tyagi, A. K. *J. Phys. Chem. C* **2012**, *116*, 12462.
(31) Liu, M.; Qiu, X.; Miyauchi, M.; Hashimoto, K. *Chem. Mater.* **2011**, *23*, 5282.
(32) Hoang, S.; Berglund, S. P.; Hahn, N. T.; Bard, A. J.; Mullins, C. B. *J. Am. Chem. Soc.* **2012**, *134*, 3659.
(33) Zuo, F.; Wang, L.; Wu, T.; Zhang, Z.; Borchardt, D.; Feng, P. *J. Am. Chem. Soc.* **2010**, *132*, 11856.
(34) Yu, Y.; Wu, K.; Wang, De. *Appl. Phys. Lett.* **2011**, *99*, 192104.
(35) Xia, J.; Masaki, N.; Jiang, K.; Yanagida, S. *J. Phys. Chem. B* **2006**, *110*, 25222.
(36) Su, J.; Zou, X.-X.; Li, G.-D.; Li, L.; Zhao, J.; Chen, J.-S. *Chem. Commun.* **2012**, *48*, 9032.
(37) Zhao, Q.; Wu, P.; Li, B. L.; Lu, Z. M.; Jiang, E. Y. *J. Appl. Phys.* **2008**, *104*, 073911.
(38) Guillemot, F.; Porté, M. C.; Labrugère, C.; Baquey, C. *J. Colloid Interface Sci.* **2002**, *255*, 75.
(39) Khomenko, V. M.; Langer, K.; Rager, H.; Fett, A. *Phys. Chem. Miner.* **1998**, *25*, 338.
(40) Li, M.; Hebenstreit, W.; Diebold, U. *J. Phys. Chem. B* **2000**, *104*, 4944.
(41) Lee, J.; Zhang, Z.; Deng, X.; Sorescu, D. C.; Matranga, C.; Yates, J. T., Jr. *J. Phys. Chem. C* **2011**, *115*, 4163.
(42) (a) Bahramia, B.; Khodadadi, A.; Kazemeini, M.; Mortazavi, Y. *Sens. Actuators, B* **2008**, *133*, 352. (b) Yamaura, H.; Tamaki, K.; Moriya, J.; Miura, N.; Yamazoe, N. *J. Electrochem. Soc.* **1997**, *144*, L158. (c) Oliaeea, S. N.; Khodadadia, A.; Mortazavib, Y.; Alipoura, S. *Sens. Actuators, B* **2010**, *147*, 400. (d) Yamaura, H.; Jinkawa, T.; Tamaki, J.; Moriya, K.; Miura, N.; Yamazoe, N. *Sens. Actuators, B* **1996**, *35*−*36*, 325. (e) Sedghi, S. M.; Mortazavi, Y.; Khodadadi, A. *Sens. Actuators, B* **2010**, *145*, 7. (f) Yamaura, H.; Tamaki, J.; Moriya, K.; Miura, N.; Yamazoe, N. *J. Electrochem. Soc.* **1996**, *143*, L36. (g) Savagea, N. O.; Akbarb, S. A.; Duttaa, P. K. *Sens. Actuators, B* **2001**, *72*, 239.
(43) (a) Sun, C.; Rajasekhara, S.; Chen, Y.; Goodenough, J. B. *Chem. Commun.* **2011**, *47*, 12852. (b) Choi, S. H.; Hwang, I. S.; Lee, J. H.; S. Oh, G.; Kim, I. D. *Chem. Commun.* **2011**, *47*, 9315. (c) Chen, D.; Hou, X.; Wen, H.; Wang, Y.; Wang, H.; Li, X.; Zhang, R.; Lu, H.; Xu, H.; Guan, Sh.; Sun, J.; Gao, L. *Nanotechnology* **2010**, *21*, 035501. (d) Bai, S.; Hu, J.; Li, D.; Luo, R.; Chen, A.; Liu, C. C. *J. Mater. Chem.* **2011**, *21*, 12288. (e) Chaudhari, G. N.; Bende, A. M.; Bodade, A. B.; Patil, S. S.; Sapkal, V. S. *Sens. Actuators, B* **2006**, *115*, 297.
(44) (a) Polleux, J.; Gurlo, A.; Barsan, N.; Weimar, U.; Antonietti, M.; Niederberger, M. *Angew. Chem.* **2006**, *118*, 267. (b) Liao, L.; Zhang, Z.; Yan, B.; Zheng, Z.; Bao, Q.; Wu, L. T.; Li, C. M.; Shen, Z. X.; Zhang, J. X.; Gong, H.; Li, J. C.; Yu, T. *Nanotechnology* **2009**, *20*, 085203. (c) Du, X.; Du, Y.; George, S. M. *J. Phys. Chem. A* **2008**, *112*, 9211. (d) Al-Kuhaili, M. F.; Durrani, S. M. A.; Bakhtiari, I. A. *Appl. Surf. Sci.* **2008**, *255*, 3033. (e) Chang, S. J.; Hsueh, T. J.; Chen, I. C.; Huang, B. R. *Nanotechnology* **2008**, *19*, 175502. (f) Comini, E.; Yubao, L.; Brando, Y.; Sberveglieri, G. *Chem. Phys. Lett.* **2005**, *407*, 368. (g) Park, J. A.; Moon, J.; Lee, S. J.; Kim, S. H.; Zyung, T.; Chu, H. Y. *Mater. Lett.* **2010**, *64*, 255. (h) Neri, G.; Bonavita, A.; Micali, G.; Rizzo, G.; Callone, E.; Carturan, G. *Sens. Actuators, B* **2008**, *132*, 224. (i) Parka, J.; Shena, X.; Wang, G. *Sens. Actuators, B* **2009**, *136*, 494.